Asian Journal of Water, Environment and Pollution, Vol. 12, No. 2 (2015), pp. 1–11.

Environmental Magnetism of Roadside Soil Contamination in the Restricted Bijyodaira Area of Mt. Tateyama, Toyama, Japan

Kazuo Kawasaki*, Keiji Horikawa and Hideo Sakai

Section of Earth and Environmental Systems, University of Toyama
Toyama-shi, Toyama, Japan. 930-8555
✉ kkawasak@sci.u-toyama.ac.jp

Received January 26, 2015; revised and accepted March 3, 2015

Abstract: Environmental magnetic techniques have been shown to be highly useful for investigating roadside pollution in Europe, North America and Asia. However, no studies have reported such magnetic monitoring in Japan. Here we report environmental magnetic results along the Tateyama-Kurobe Alpine route at the Bijyodaira area of Mt. Tateyama in Toyama, which is part of the Special Protection Zone of the Chubu Sangaku National Park. In-field susceptibility measurements from 17 sites (297 points) as well as in-laboratory susceptibility measurements from six sites (75 surface and auger core soil samples) show higher susceptibilities near the roadside and a positive correlation between the susceptibility and heavy metal contents. Also, the concentration of the magnetic minerals and associated heavy metals near the surface shows less vertical downward migration of these materials below 15 cm from surface. Rock magnetic analyses indicate that: (a) the major magnetic minerals are pseudosingle- and multi-domain magnetite and/or titanomagnetite; (b) the closer the road side, the more anthropogenic magnetite is present; and (c) most pollutants derived from the vehicles are deposited within a few metre distances from the road through the area. Overall, the results show that environmental magnetic techniques are suitable for studying pollution associated with vehicle traffic elsewhere in Japan.

Key words: Environmental magnetism, magnetic properties, roadside soil contamination, national park, Japan.

Introduction

Environmental magnetic techniques have been shown to be highly useful for investigating industrial pollutants and other atmospheric aerosols (e.g. Evans and Heller, 2003; Magiera et al., 2006). Beckwith et al. (1990) reported a magnetic investigation of pollution in an urban highway environment in London, England, and concluded that the dominant source of the pollution is closely associated with motor vehicles. Matzka and Maher (1999) collected leaves from roadside trees in England and found that leaves from rural settings were ten times less magnetic than those collected near busy urban roads. Conversely, Kletetschka et al. (2003) found that forest-facing tree-bark shows a higher magnetic susceptibility value than road-facing tree-bark when collected close to a highway and interpreted this observation to be due to more moisture on the forest-facing tree trunk. Magnetic susceptibility measurements of topsoil have proven to be a highly efficient method to study traffic pollutants along roadsides (e.g. Hoffmann et al., 1999; Gautam et al., 2004; Schmidt et al., 2005; Shi and Cioppa, 2006). Similarly, magnetic investigations of road dust collected by ground sweeping with a brush have shown the effective method to investigate the spatial and temporal distribution of anthropogenic materials in urban areas (Kim et al., 2007; Kim et al., 2009; Yang et al., 2010). However, no systematic

*Corresponding Author

magnetic investigation on the spatial distribution of magnetic properties along roadsides has been done in Japan. Torii (2005) pointed out two major reasons for this paucity: (a) there are lots of volcanos in Japan that supply great amounts of magnetically-enhanced fly ashes that blind out the pollution-originated magnetic signals; and (b) the dense population in Japan causes substantial amounts of magnetic noise. Here we present the first environmental magnetic studies for Mt. Tateyama in Toyama, which is part of the Special Protection Zone of the Chubu Sangaku National Park in Japan (Figure 1A). Our aims are to show that environmental magnetic investigations can be an effective tool in Japan and to evaluate the roadside pollution derived from vehicles.

Methodology

Site Description

Mt. Tateyama is located in eastern Toyama prefecture, Japan. The Midagahara and Dainichidaira areas within the Mt. Tateyama area joined the Convention on Wetlands of International Importance, especially as Waterfowl Habitat in 2012. Mt. Tateyama has been known as one of the major sacred mountains in Japan and therefore the area has been relatively undisturbed since ancient times. In addition, the area is restricted to vehicular traffic and other construction as a part of the Special Protection Zone. The only available road at Mt. Tateyama is the Tateyama-Kurobe Alpine sightseeing route opened in 1971. This route is only open from mid-April to the end of November because of heavy snowfall in the winter season. Only authorised vehicles have been allowed to drive the route in order to protect the environment since it was opened. The Tateyama-Kurobe Kanko Inc. is the major public transport company on the route and it has been changing the buses to low-emission hybrid diesel engines since 1999. So far 24 of its 38 buses have been replaced. However, a considerable number of non-hybrid diesel engine buses of other companies take the route as well as utility cars that maintain facilities for tourists and construction (Kume et al., 2009). The number of vehicles is recorded by the Toyama prefecture's public road corporation. The number of tourist buses in 2012 was 2589.

Several investigations have been reported that evaluate the effects of vehicles on the surrounding environment (Kawano, 1999; Kume et al., 2009). Kawano (1999) reported that most *Fagus crenata*, or Japanese beech, trees near the route suffered from visible injury and other symptoms of decline that were not caused by pests or disease. Kume et al. (2009) reported on the effects of air pollution on the growth of mountain trees in the Bunadaira area of Mt. Tateyama. They concluded that the decline of *Fagus crenata* trees along the route was not caused significantly by the air pollution emitted from the passing buses. They suggested that both regional and long-range transported air pollution had affected the growth of these trees. Recently, Horikawa et al. (2013) reported evidence of historical changes in soil acidification in a Tateyama cedar tree at Bijodaira, Mt. Tateyama. They concluded that the significant increases of Ca concentrations accompanied the local road building activities along the Alpine route. Our study area is in the Bijodaira area and is between the Bijodaira station at 977 m above sea level (asl) and Bunadaira at ~1197 m asl (Figure 1B). The annual precipitation at the Bijodaira area is estimated to be 2000 to 3000 mm and the maximum snow depth is ~3.5 m. The major vegetation is natural *Fagus crenata* trees (Kume et al., 2009). Mt. Tateyama is a composite volcano which began its activity in the Pliocene. The entire Bijyodaira area consists of andesitic flows (Harayama et al., 2000) and the soils are classified as "mountain dark-brown coniferous-forest" soils (Horikawa et al., 2013).

In-field Measurements

In-field volume magnetic susceptibility was measured using a Bartington MS2-D magnetic susceptibility meter and probe. The MS2-D probe can reach to a depth of 10 cm (Lecoanet et al., 1999). The susceptibility provides an estimate of the total magnetic content. At each measurement point, five measurements were done to ensure repeatability and representativeness. In addition air measurements were made before and after each measurement on topsoil to ensure compensation for instrument drift. The in-field susceptibility of the topsoil was measured at three sites in 2012 and 14 sites in 2013 (Figure 1B). All measured sites except site A are along the Tateyama Kurobe Alpine route from the Bijyodaira station to the Bunadaira. Site A is a control point which is ~120 m away from the roadside. Except sites 4 and 6 where only soils are sampled, a survey line was set up at the 14 remaining numbered sites (1-3, 5, 7-16) from 0 m up to 10 m from the road. Note that the 0 m point at each site is set at 0.8 m from the roadside gutter to avoid the effect of gutter's extremely high susceptibility. For site B, a survey line was set up from 0 m to 25 m. Site C was set up to examine a dense grid of measurements, i.e. the eight survey lines had a 0.5 m spacing along the Alpine route (sites C-1 to C-8). For site C, seven survey lines extended from 0 m to 5 m

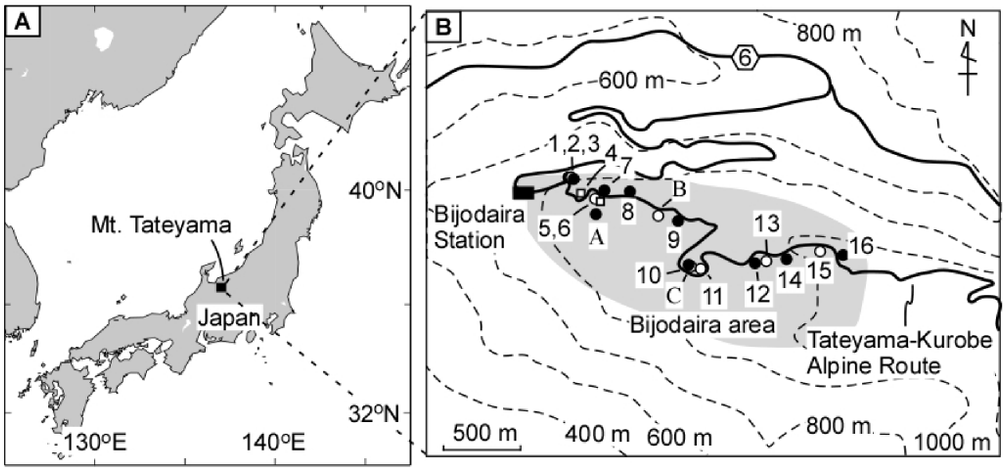

Figure 1: (A) Regional map with the solid box indicating the study area. (B) the Bijodaira area is shown by grey hatches. Sites A to C were studied in 2012 and sites 1 to 16 were studied in 2013. Solid circles and open circles denote the sites where only in-field measurements and where both in-field and in-laboratory measurements were done, respectively. Open squares denote sites where only topsoils were collected.

from the road and one line extended set from 0 m to 40 m. The spacing of survey points on each line were set in three intervals in order to determine the distribution of polluted materials derived from vehicles: (a) 0.25 m spacing between 0 and 1 m; (b) 0.5 m spacing between 1 and 5 m; and (c) 1 m spacing between 5 and 10 m. For sites B and C-1, additional measurements were carried out at 15 and 25 m and at 20 and 40 m, respectively.

Sampling

A total of 56 topsoil samples (0-1 cm depth) were collected at selected sites (Figure 1B). Also two cores with depths of 0.45 m and 0.5 m were collected at 1.5 m from roadside of site B and 0 m from roadside of site C, respectively. The cores were collected using a soil auger and divided into 5 cm lenghts, resulting 10 and 9 samples for sites B and C, respectively. A total of 67 soil samples were measured to obtain their pH. The soil pH (H_2O) of the roadside samples at sites B and C represent 4.5±0.4 (n = 2) and 5.3±0.2 (n = 7), respectively. More detailed methodologies and results for the soil pH (H_2O) are reported in Horikawa et al. (2013). All samples were dried in air and then coarse grains, roots and leaves were removed by passing the soil through a 1 mm sieve. Prepared soils were then put into 7 cc non-magnetic plastic cubes. The cubes were weighed before and after putting in the specimens. All magnetic measurements of the 75 samples were conducted in the rock magnetic laboratories at the University of Toyama.

We conducted geochemical analyses of 40 samples collected at sites B and C. Exchangeable base cations (Na, Mg, Al, Ca, Mn, Ba, Sr, Zn, Cu and Cd) in the soil samples were extracted using 1 mol/L, pH 7.0 ammonium acetate (Tamapure AA-100, Tama Chemical Ltd) after running for ca. 14 h in a shaker at room temperature with a mass to volume ratio of ca. 2.5 g: ca. 35 mL (Chen et al., 2010). The diluted extracted solution was measured using a quadrupole inductively coupled plasma mass spectrometry (ICP-MS, HP4500, Agilent Technologies) at the University of Toyama.

Results

In-field Susceptibility

In-field susceptibility values vary by two orders of magnitude, ranging from -0.8×10^{-5} to 226.2×10^{-5} SI. The median susceptibility was 20.9×10^{-5} SI (number of measurement points (N) = 297, quartiles: $Q_1 = 9.2 \times 10^{-5}$, $Q_3 = 38.9 \times 10^{-5}$). Higher susceptibility values than the median susceptibility were mostly observed near the roadside. The susceptibility decay curves show rapid decreases within 2 m from the road for most lines (Figure 2). The susceptibility for the control point, site A, is 25.6×10^{-5} SI. The susceptibilities for site B at 15 m and 25 m are 4.8×10^{-5} SI and 6.6×10^{-5} SI, respectively. The susceptibilities for site C-1 at 20 m and 40 m are 16.0×10^{-5} SI and 5.0×10^{-5} SI, respectively. At site C, high susceptibilities are also observed between 2.5 and 4 m from the road.

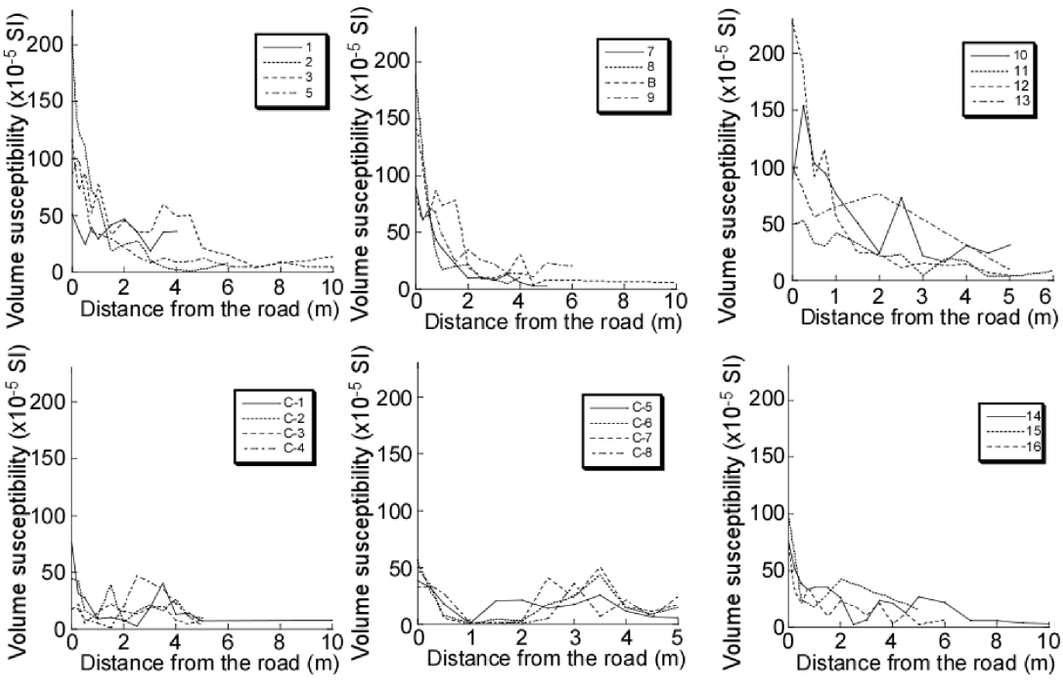

Figure 2: In-field volume susceptibility curves for all survey lines.

In-laboratory Measurements

Susceptibility

Room-temperature low-field volume susceptibility (*k*) was measured with an MS2-B Bartington susceptibility meter. Then the specimens' volume susceptibilities were divided by density to calculate the mass susceptibility (χ). Mass magnetic susceptibility measurements in the laboratory on all collected samples were similar in trend to the in-field volume susceptibility measurements (Figure 3), indicating that higher susceptibility values observed by in-field measurement were not likely due to measurement errors such as presence of higher susceptible gravels.

The vertical profiles of mass susceptibilities are not corresponding although they are trends (Figure 4). The mass susceptibilities for site B increase with the depth. Conversely the mass susceptibilities for site C increase up to 15 cm and then start to decrease.

The percentage frequency-dependent susceptibility ($\chi_{FD} = 100(\chi_{LF} - \chi_{HF})/(\chi_{LF})$) ($\chi_{LF}$ = 460 Hz and χ_{HF} = 4600 Hz) indicates the presence of grains lying at the stable single domain (SD)/superparamagnetic (SP) boundary. For the SP/SD grain sizes, χ_{FD} lies in the

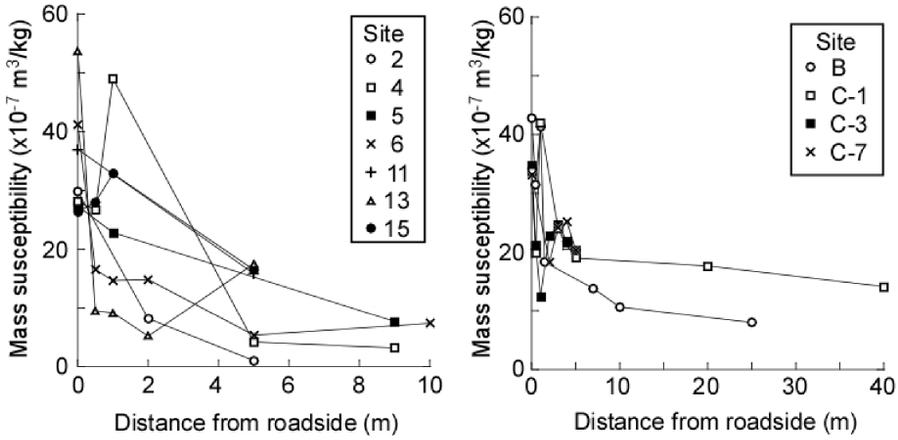

Figure 3: Mass susceptibility curves for top soils.

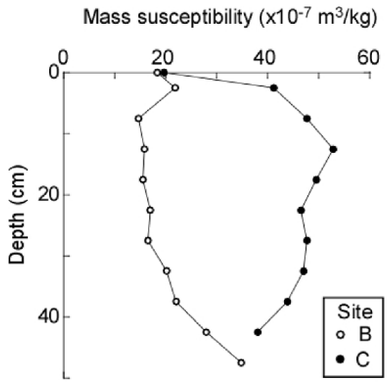

Figure 4: Vertical profiles of mass susceptibilities for sites B (○) and C (●). The cores for sites B and C were taken at distances of 1.5 m and 0 m from the roadside, respectively.

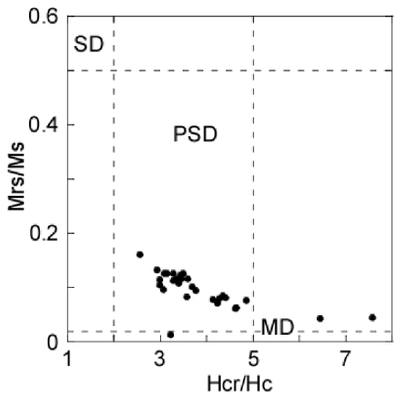

Figure 5: Day plot for the selected topsoil samples.

range of 7-14%, while for the multidomain (MD) grains χ_{FD} is <5-6% (Dearing et al., 1996). Almost all measured samples (97%) have less than 6% of frequency-dependent susceptibility, indicating that the soils at the study area are not dominated by frequency-dependent SP grains (Maher, 1988). In addition, 76% samples have less than 2% of frequency-dependent susceptibility, indicating the dominance of frequency-independent coarse MD or PSD grains in the soils.

Hysteresis

From hysteresis loops and backfield demagnetization curve measurements, two ratios, M_{rs}/M_s and H_{cr}/H_c, can be obtained and illustrated on a Day plot (Day et al., 1977; Dunlop, 2002a; Dunlop, 2002b). The Day plot allows the ferrimagnetic grain size to be estimated. Hysteresis loops were generated by subjecting a small sample to a large magnetic field H_{max} = 500 mT. Hysteresis loops and backfield demagnetization as well as isothermal remanent magnetization (IRM) were obtained for selected specimens using a Lake Shore Cryotronics PMC MicroMag AGM model 3900. Thirty representative specimens, each with the weight of ~10 mg, were chosen for the hysteresis analyses and subsequent IRM acquisition tests. The averaged value of three measurements was used to determine specimen's hysteresis loops. On a Day plot, most data points fall in the pseudosingle-domain (PSD) region whether close to or far from the road (Figure 5). There are two possibilities for this result: (a) dominance of PSD grains, or (b) a mixture of multi-domain (MD) and single-domain (SD) grain size. However, H_c values of all samples are less than 12 mT, and SD magnetite has higher H_c values than MD minerals (Evans and Heller, 2003), indicating that larger grains (PSD/MD) are dominant in the soils. The IRM test shows that all measured samples are entirely saturated by ~300 mT, indicating that the main remanence carrier is MD magnetite (Figure 6) (Symons and Cioppa, 2000).

Temperature Dependence of Susceptibility

The thermal alteration of spontaneous magnetization is a fundamental magnetic property because it depends only on a ferromagnet's composition and crystalline structure (Dunlop and Özdemir, 1997). This property can be used to identify reliably the magnetic minerals carrying the magnetism of specimens in their diagnostic temperature range and preferable atmosphere. The susceptibility dependence on temperature curves for 12 selected specimens from room temperature to 700°C were measured on an AGICO Kappabridge KLY-3 with

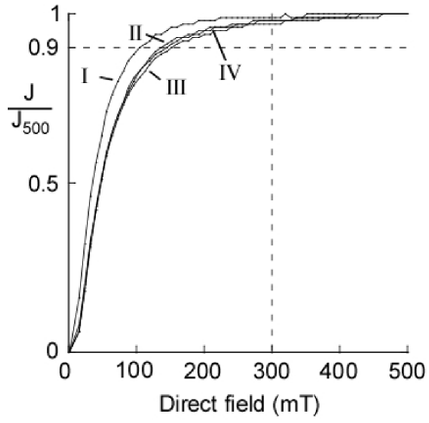

Figure 6: IRM acquisition curves for representative samples of: (I) 0 m at site 5; (II) 0 m at site 11; (III) 9 m at site 5; and (IV) 5 m at site 11. J_{500}, intensity value at 500 mT.

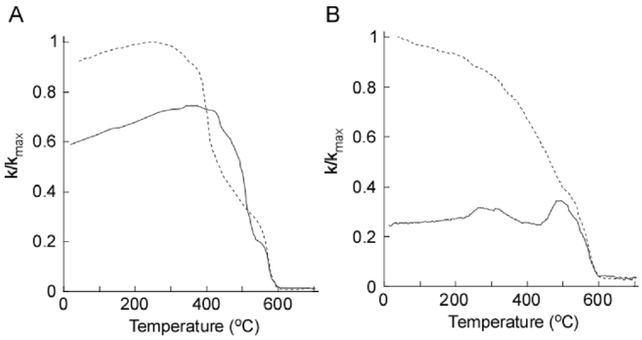

Figure 7: Temperature dependence of susceptibility curves for example samples: (A) 0 m at site 4 and (B) 5 m at site 4. Solid and dashed lines show heating and cooling curves, respectively. The curves were measured with the samples in an Ar atmosphere.

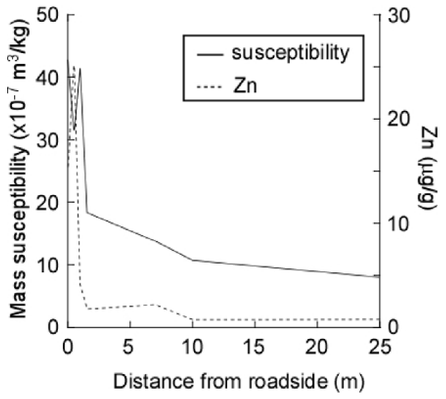

Figure 8: Mass susceptibility and zinc concentrations for surface soils at site B, showing corresponding variations.

a CS-3 high-temperature furnace in an Ar atmosphere. Well-defined Curie temperatures were observed at ~540 and ~580°C for the soil samples, indicating both titanomagnetite and magnetite, respectively as the predominant magnetic carriers. A continuous intensity decrease to ~400°C is observed for the soils taken at >5 m from the roadside, indicating titanomagnetite (Figure 7). The sudden intensity increase around 450-500°C records the oxidation in the oven of iron sulphides such as pyrite to magnetite (Dunlop and Özdemir, 1997).

Geochemical Analyses

Measured concentration data for 10 elements is shown in Table 1. In this study, we mainly focus on zinc (Zn) because it is one of the heavy metals embedded in tire dust and traffic-related materials such as brake dust and tire tread (e.g., Fukuzaki et al., 1986). For the soil samples collected at sites B and C, the Zn concentrations show significant correlations to some trace metals such as Cd (R = 0.78), Ba (R = 0.70), and Cu (R = 0.68). Further, the Cd-Zn and Cu-Zn plots also show that the Zn concentrations of surface soils represent relatively higher values compared to the deeper soil sediments, indicating that Zn is enriched in the surface soils. Surface soil sediments at <1 m from the roadside are marked by higher concentrations in Zn compared to the surface sediments farther away from the Alpine route (Figures 9a and 9b). This decreasing trend of Zn concentrations with the distance is observed at site B in a transect from the roadside to the grove (0-25 m) and shows a similar decay curve to the mass susceptibility curve (Figure 8).

Discussion

Vertical Profiles

The vertical distribution of susceptibility in soils is important for discriminating between the anthropogenic and lithogenic contributions to topsoil susceptibility. Magiera et al. (2006) reported the anthropogenic enhancement of susceptibility in topsoil and the second enhanced layer below 15-20 cm depth due to pedogenesis based on ~600 soil core profiles in Central Europe. Kapička et al. (2011) reported an experimental study of the vertical migration of power-plant fly ash into sands using magnetic methods and they concluded that the fly ash particles when deposited on fine sand could only move a few millimetres under the surface even after repeated rain simulation. Conversely, Sapkota et al. (2012) reported a controlled experimental study using magnetite powder on soil and concluded that magnetite could migrate vertically downwards at a rate of ~14 cm/year due to rainwater infiltration. Recently Lourenço et al. (2014) reported magnetic and geochemical characterisation of six soil profiles collected from polluted and unpolluted area in Portugal and found that the magnetic enhancement between 0 cm and 15 cm is related to the deposition of industrial emissions and the synthesis of magnetite/maghemite during pedogenic processes, including biologically induced mineralization. They concluded that the boundary between clean soil and polluted soil is at the depth of 10-20 cm based on the susceptibility and heavy metal variation. The vertical distribution

of susceptibility for site B shows relatively higher susceptibility within 0-5 cm from surface (Figure 4), indicating that the anthropogenic materials are located near the surface with minimal mixing or downward migration. The increase of susceptibility from 25-30 cm is likely the results of influence of magnetically enhanced parent rocks (Magiera et al., 2006).

Conversely, the mass susceptibility for site C increases between 0 cm and 10-15 cm and then gradually decreases below 10-15 cm (Figure 4). This result is similar to previously reported susceptibility distribution of polluted area (Lourenço et al., 2014). The observed higher susceptibly is likely caused by more influx of magnetic minerals related to vehicle emissions because the core of site C is closer to the roadside. Our results show that there is less downwards migration of magnetic minerals or of the anthropogenic heavy metal elements (Table 1; Figures 4 and 9a, b), indicating that most anthropogenic materials are located in a stable position near surface and the boundary between polluted soil and unpolluted soil at the depth of 10-15 cm. Therefore, standard top-soil susceptibility mapping of the Bijyodaira area using MS-2D probe that could reach to a depth of 10 cm is highly likely to be reliable and fully representative.

The Relationship between Susceptibilities and Distance from the Road

Mass susceptibility measured on soil samples in the laboratory is consistent with in-field volume susceptibility (Figures 2 and 3), indicating that in-field susceptibility measurements are an effective method to provide primary information for the distribution of roadside dust without any surface destruction in the Bijyodaira area. All sites except site 5 have similar susceptibility decay curves, i.e. the peaks of susceptibility values appear within 0.25 m from the road and the values show rapid decay between the peak and 2 m from the road. The results imply that the susceptibility values decrease to almost basal values at ≥5 m. The median mass susceptibility for the 17 samples collected ≥5 m from the roadside is 13.8±6.4 ($\times 10^{-7}$ m^3/kg). This background threshold value should prove useful for identifying regional pollution in the Bijodaira area. In addition, the zinc content in the soil shows a positive correlation with susceptibility (Pearson's correlation coefficient, $r = 0.606$, $P < 0.05$) (Figure 8). Hence the magnetic susceptibilities of the topsoils likely provide a reliable proxy for the distribution of anthropogenic pollutant from vehicles. Also the results indicate that the anthropogenic pollutants are deposited mainly within <2 m from the road and do not flow into the surrounding forests. These results are coincident with previously reported results that the anthropogenic materials derived by automobiles are deposited within 5 m with the peak between 0 m and 1 m (Hoffmann et al., 1999). Conversely, the site A control point shows a higher mass susceptibility of 41.7 ($\times 10^{-7}$ m^3/kg) than the defined background threshold value. Since this site is located ~120 m away from the roadside, the effect of pollutant derived from vehicles should be negligible. The higher susceptibility of control point could be the results of natural spatial variability in susceptibility and may be caused by the effect of regional and/or long-range transport of air pollution.

Kim et al. (2012) reported magnetic properties of atmospheric particles from an air sampler station in Korea and concluded that the temporal variation of magnetic concentration is likely caused by the increases of anthropogenic particulates derived by Asian dust storm. Coastal areas along the Sea of Japan, including Mt. Tateyama, have been exposed to large amounts of atmospheric acidic pollutants delivered by the westerly jet stream and northwesterly winter monsoons (Nagashima et al., 2007; Watanabe et al., 2011). Although such acidic pollutants may play an important role for the magnetic susceptibility of soils in the forest, we have only the one data, which is certainly not enough to discuss the effect of air pollution from long-range transportation from the Asian continent. Nonetheless, the similar spatial distributions of mass susceptibility at all sites except control point, i.e., the higher susceptibility near the roadside and its decrease with distance from the roadside (Figure 3) indicate that these acidic pollutants from regional or faraway sources have little effect to the topsoil near the roadside and the natural spatial variability in susceptibility is not significant along the topsoil within ~40 m from the roadside. In addition, Magiera et al. (2006) suggested that the susceptibility measurements can detect the anthropogenic effect of soils developed on basaltic rocks. Our results show that anthropogenic effect from vehicle traffic can be observed in soils developed on andesitic flows at least near the roadside area.

Magnetic Minerals

Based on the IRM acquisition, Day plot, frequency-dependent susceptibility and the temperature dependence of susceptibility tests, the main magnetic minerals in the soils are PSD-MD magnetite and titanomagnetite. Titanomagnetite is commonly found in igneous and metamorphic rocks. Given that the entire Bijyodaira area

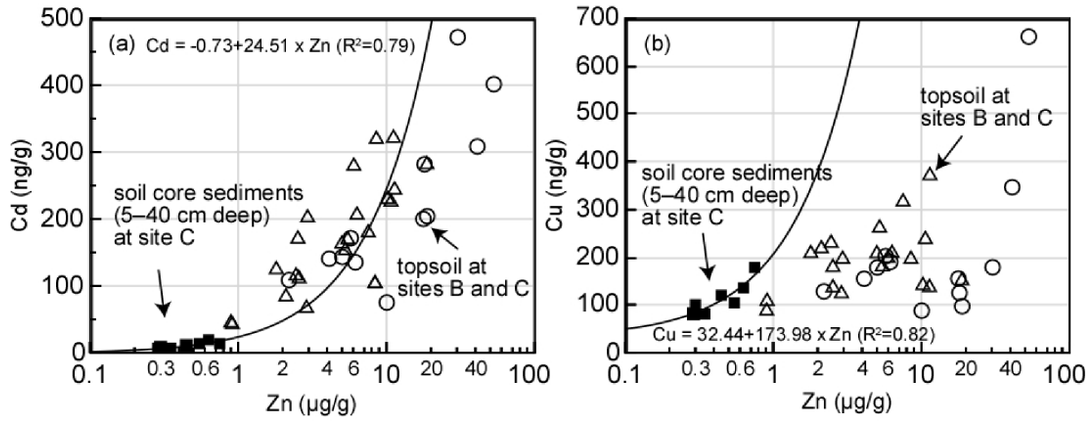

Figure 9: Plots of: (a) Cd and Zn concentration; and (b) Cu and Zn concentration. Filled squares indicate soil core sediments at site C, whereas open symbols indicate surface soil sediments at sites B and C. Roadside surface soils from within 1 m of the roadside are open circles and open triangles are from surface soil samples taken from a distance of more than 1 m. Regression curves in each plot are derived from soil core sediment data at site C, suggesting that some surface soil sediments, especially near roadside, are extremely enriched in anthropogenic Zn that cannot be explained by the natural Cd/Zn and Cu/Zn ratios observed in deeper soil that is little affected by anthropogenic pollution

is underlain by andesitic flows (Harayama et al., 2000), a reasonable conclusion is that the soil's titanomagnetite originated from the weathering of the lava flows. Magnetite is also abundant in most other igneous rocks. However, because the common anthropogenic magnetic minerals include magnetite (e.g. Evans and Heller, 2003), both natural and anthropogenic origins are possible for the magnetite in the soils of the Bijyodaira area. The cooling curves for the temperature dependence of susceptibility yielded irreversible enhancement of the susceptibility after heating, suggesting that new magnetic minerals with higher susceptibility values have been created during the heating processes (Figure 7a, b). The averaged susceptibility value of the six selected samples with higher susceptibilities of >20 ($\times 10^{-7}$ m^3/kg) after the heating and cooling process is 1.6±0.5 times greater than before heating. Conversely, the averaged susceptibility value of the six selected samples with weaker susceptibilities of <20 ($\times 10^{-7}$ m^3/kg) after heating and cooling process is 4.4±1.7 times greater than their values before heating.

These contrasting results indicate that the soils with higher magnetic susceptibility have suffered less formation of new magnetic minerals on heating and cooling than the ones with weaker susceptibility. The significant peak around 500°C (Figure 6B) is likely caused by either the neoformation of magnetite through the transformation of iron-containing silicates and/or clays (Dunlop and Özdemir, 1997) or transformation of goethite reacting with organic matter and being reduced into maghemite (Hanesch et al., 2006). The weaker magnetic susceptibilities are found far from the roadside. Thus the anthropogenic magnetic minerals such as magnetite are less likely to be present in these samples and, therefore, the amounts of natural iron-containing silicates or goethite in the soil are relatively much greater than in the soil near the roadside. The significant difference of these ratios observed in the temperature dependence of susceptibility indicates that the dominant magnetic mineral in soils near the roadside is anthropogenic magnetite, and thus this property could be useful for distinguishing between polluted and unpolluted soils. Sheng-gao et al. (2005) reported an environmental magnetic study of vehicle emission particulate samples taken from exhaust pipes and they concluded that the main magnetic mineral in the samples was MD magnetite with a notable absence of SP grains.

In addition, Yang et al. (2010) reported that the main magnetic carrier of road dust collected by sweeping with a brush is a coarse grained magnetite. The magnetic grains of our samples are mostly PSD to MD in size with relatively few SP grains, suggesting that anthropogenic magnetic minerals are more abundant and dominant than the natural magnetic minerals formed by pedogenesis (Mullins, 1977). The iron-rich magnetic materials result from rusting of the bodywork, wear of the moving parts and ablation from the interior of the exhaust system (Evans and Heller, 2003). The Zn concentration shows a positive correlation with the magnetic susceptibility and the major sources of Zn would be tire tread and

Table 1. Exchangeable base cations data (Na, Mg, Al, Ca, Mn, Ba, Sr, Zn, Cu and Cd) in the soil samples from sites B and C

Site/type/distance or depth	*Na (μg/g)*	*Mg (μg/g)*	*Al (μg/g)*	*Ca (μg/g)*	*Mn (μg/g)*	*Ba (μg/g)*	*Sr (μg/g)*	*Zn (μg/g)*	*Cu (ng/g)*	*Cd (ng/g)*
B / surface soil / 0 m	386.90	966.23	139.56	3675.01	5.76	5.76	3.95	2.20	128.8	108.9
B / surface soil / 0.5 m	72.76	612.94	99.24	3746.69	3.14	9.60	18.10	2.54	139.6	172.6
B / surface soil / 1 m	198.06	482.79	130.21	188.91	3.16	2.21	0.98	0.91	111.1	44.4
B / surface soil / 1.5 m	274.91	442.00	131.57	39.53	3.61	1.48	0.29	0.90	90.1	46.6
B / surface soil / 7 m	321.37	2166.64	7.34	13497.33	67.46	43.90	31.63	17.75	155.8	200.3
B / surface soil / 10 m	417.33	2552.59	11.16	17668.31	150.11	49.08	42.47	30.26	179.3	471.9
B / surface soil / 25 m	258.27	1064.13	24.89	4904.31	9.55	7.72	4.74	5.04	178.9	143.4
C-1 / surface soil / 0 m	265.96	796.23	93.19	3194.82	67.13	8.07	3.67	5.74	202.7	171.6
C-1 / surface soil / 1 m	390.96	929.16	38.27	2500.07	67.06	20.50	3.42	6.17	190.5	135.5
C-1 / surface soil / 2 m	463.85	2684.54	62.93	15571.59	272.17	22.21	30.47	11.19	140.5	322.4
C-1 / surface soil / 4 m	382.37	1552.23	102.80	5323.77	176.91	9.68	13.47	6.02	198.8	280.7
C-1 / surface soil / 5 m	641.62	1802.16	88.07	5902.12	220.59	21.24	17.29	6.35	212.2	207.7
C-1 / surface soil / 20 m	409.49	811.85	104.63	223.43	34.75	3.52	1.23	1.81	209.5	126.4
C-1 / surface soil / 40 m	1318.37	2640.61	17.73	787.15	12.60	8.49	6.74	8.56	197.9	321.3
C-3 / surface soil / 0 m	288.83	801.70	18.78	3240.47	56.87	7.67	3.43	4.11	155.4	140.9
C-3 / surface soil / 0.5 m	391.59	1927.11	10.88	10789.82	182.87	33.47	26.35	18.07	125.7	282.0
C-3 / surface soil / 1 m	634.90	1473.83	14.16	5908.48	144.78	3.90	15.48	18.75	152.5	282.8
C-3 / surface soil / 2 m	319.13	723.47	118.63	2424.79	74.52	5.01	2.04	2.54	181.8	113.2
C-3 / surface soil / 3 m	472.72	835.07	92.62	536.56	106.14	5.82	1.82	2.96	198.6	205.1
C-3 / surface soil / 4 m	665.16	1368.15	120.51	3926.91	59.45	14.33	2.87	2.90	126.7	69.5
C-3 / surface soil / 5 m	770.87	2502.72	142.75	12466.46	147.63	7.38	8.49	5.04	209.0	163.5
C-5 / surface soil / 0 m	1771.77	9990.95	22.92	47899.60	376.83	27.87	82.18	53.03	661.9	401.7
C-5 / surface soil / 0.5 m	1361.29	9771.55	14.37	51787.09	423.19	36.29	102.80	41.01	346.8	308.6
C-5 / surface soil / 2 m	410.50	1075.22	127.27	662.33	98.62	5.13	2.26	7.51	318.7	181.4
C-5 / surface soil / 3 m	635.27	910.08	103.35	2157.20	91.73	3.94	1.68	2.47	232.1	116.1
C-5 / surface soil / 4 m	993.86	1951.66	112.59	5531.40	120.19	5.31	12.21	5.24	263.7	155.0
C-5 / surface soil / 5 m	1896.21	4043.19	28.44	16679.11	224.12	25.44	33.99	10.64	238.8	227.0
C-7 / surface soil / 0 m	408.46	1626.36	11.64	9454.41	60.18	26.86	19.36	18.85	97.7	204.4
C-7 / surface soil / 2 m	602.79	3351.70	39.25	9128.43	289.31	24.93	21.51	10.26	144.6	230.7
C-7 / surface soil / 3 m	465.61	1069.44	170.56	650.74	78.71	3.75	1.71	2.11	219.3	85.9
C-7 / surface soil / 4 m	1494.52	3396.75	22.43	7370.52	478.36	9.61	6.64	11.44	372.9	245.8
C-7 / surface soil / 5 m	829.78	1679.27	14.34	4699.26	300.50	6.38	4.26	5.48	182.1	171.0
C-5@0 m / vertical / 0-5 cm	333.65	2394.25	3.55	12690.74	103.72	8.89	25.19	10.05	88.5	75.4
C-5@0 m / vertical / 5-10 cm	29.07	39.94	54.44	210.10	1.06	4.93	0.89	0.30	101.7	8.1
C-5@0 m / vertical / 10-15 cm	125.77	132.27	35.45	230.29	1.10	12.74	1.04	0.29	81.1	5.4
C-5@0 m / vertical / 15-20 cm	133.77	27.91	62.92	181.46	1.16	6.42	1.15	0.34	81.6	5.2
C-5@0 m / vertical / 20-25 cm	127.59	29.27	34.96	187.37	1.37	7.12	1.26	0.54	103.7	12.6
C-5@0 m / vertical / 25-30 cm	40.36	37.31	17.25	192.38	1.51	7.98	1.17	0.45	121.1	11.4
C-5@0 m / vertical / 30-35 cm	45.06	50.63	59.43	301.94	2.27	21.93	1.56	0.64	135.2	18.6
C-5@0 m / vertical / 35-40 cm	42.31	48.20	13.81	296.12	2.19	6.77	1.46	0.76	180.3	15.0

brake lining abrasion (e.g. Fukuzaki et al., 1986; Huhn et al., 1995). These emissions are still important even though vehicles with low-emission hybrid diesel engines become major. The maximum uses of leaded gasoline were during 1960-1965 in Japan and the amount of lead found in the Tateyama cedar tree is rapidly reduced after early 1980s in the Bijyodaira area (Horikawa et al., 2013), resulting in more clear correlation between Zn and magnetic susceptibility than between Pb concentration and susceptibility.

Conclusions

There is a positive correlation between susceptibility and heavy metal concentration in our soil samples. Vertical profiles of magnetic susceptibility indicate that any deposited anthropogenic pollutants are likely to be concentrated near the surface and are not significantly transported vertically downward below 15 cm from surface. The results of in-field susceptibility measurements along the Tateyama Kurobe Alpine route are similar to the corresponding in-laboratory susceptibility measurements, indicating that in-field measurements are useful for estimating for the distribution of roadside dust in the Bijyodaira area without any destruction of the habitat. The observed distributions of susceptibility show a higher susceptibility near the roadside that is most likely from passing vehicles, and these pollutants are mainly deposited within 2 m of the roadside. Based on rock magnetic tests, the main magnetic minerals in soils are PSD-MD magnetite and titanomagnetite with the few SP grains.

The magnetite can be both natural and anthropogenic in origin. However, anthropogenic magnetite is the dominant magnetic mineral in the soils near the roadside that have a distinctively higher susceptibility. In addition, the different susceptibility ratios produced by thermochemical alteration during the temperature-dependence of susceptibility tests for soils close to and far from the roadside could be useful for determining whether a soil is polluted or unpolluted. The test indicates the relative amounts of anthropogenic magnetite, which is unaltered by heating, and of natural iron-containing silicates and/or goethite that are reduced to generate new magnetite and/or maghemite during heating. More importantly, this study has shown that environmental magnetic methods are effective and inexpensive techniques for studying soil pollutants in Japan and, therefore, that they should be considered for application elsewhere in the country.

Acknowledgements

The authors gratefully thank: Toyama Prefecture and the Toyama District Forest Office for allowing access to the study area and permitting the soil sampling; Yoshitake Furuya, Kazuhito Hori, Ryuhei Kimura, Tomohiro Kodaira and Shinichiro Kojima for their help in field measurements; David Symons for helpful comments on an earlier draft of this manuscript; and, anonymous reviewers for helpful comments that have improved this paper. This study was partly supported by a research grant from the Japan Seaology Promotion Organization through K.K.

References

Beckwith, P., Ellis, J. and D. Revitt (1990). Applications of Magnetic Measurements to Sediment Tracing in Urban Highway Environments. *Science of the Total Environment*, **93:** 449-463.

Chen, L., Wu, F.-H., Liu, T.-W., Chen, J., Li, Z.-J., Pei, Z.-M. and H.-L. Zheng (2010). Soil Acidity Reconstruction Based on Tree Ring Information of a Dominant Species *Abies Fabri* in the Subalpine Forest Ecosystems in Southwest China. *Environmental Pollution*, **158:** 3219-3224.

Day, R., Fuller, M. and V. Schmidt (1977). Hysteresis Properties of Titanomagnetites: Grain-Size and Compositional Dependence. Physics of the Earth and Planetary Interiors, **13:** 260-267.

Dearing, J., Dann, R., Hay, K., Lees, J., Loveland, P., Maher, B.A. and K. O'grady (1996). Frequency-Dependent Susceptibility Measurements of Environmental Materials. *Geophysical Journal International*, **124:** 228-240.

Dunlop, D.J. (2002a). Theory and Application of the Day Plot (Mrs/Ms Versus Hcr/Hc) 1. Theoretical Curves and Tests Using Titanomagnetite Data. *Journal of Geophysical Research*, **107:** EPM 4-1-EPM 4-22.

Dunlop, D.J. (2002b). Theory and Application of the Day Plot (Mrs/Ms Versus Hcr/Hc) 2. Application to Data for Rocks, Sediments, and Soils. *Journal of Geophysical Research: Solid Earth (1978–2012)*, **107(B3):** EPM 5-1-EPM 5-15.

Dunlop, D.J. and Ö. Özdemir (1997). Rock Magnetism: Fundamentals and Frontiers. Cambridge University Press, Cambridge.

Evans, M. and F. Heller (2003). Environmental Magnetism: Principles and Applications of Enviromagnetics. Academic Press.

Fukuzaki, N., Yanaka, T. and Y. Urushiyama (1986). Effects of Studded Tires on Roadside Airborne Dust Pollution in Niigata, Japan. *Atmospheric Environment*, **20:** 377-386.

Gautam, P., Blaha, U., Appel, E. and G. Neupane (2004). Environmental Magnetic Approach Towards the Quantification of Pollution in Kathmandu Urban Area, Nepal. *Physics and Chemistry of the Earth, Parts A/B/C*, **29:** 973-984.

Hanesch, M., Stanjek, H. and N. Petersen (2006). Thermomagnetic Measurements of Soil Iron Minerals: The Role of Organic Carbon. *Geophysical Journal International*, **165:** 53-61.

Harayama, S., Takahashi, Y. and S. Nakano (2000). Geology of the Tateyama District. Quadrangle Series, 1:50,000. Geological Survey of Japan.

Hoffmann, V., Knab, M. and E. Appel (1999). Magnetic Susceptibility Mapping of Roadside Pollution. *Journal of Geochemical Exploration*, **66:** 313-326.

Horikawa, K., Takeda, M., Kawasaki, K. and J. Zhang (2013). Historical Changes in Soil Acidification Inferred from the Dendrochemistry of a Tateyama Cedar at Bijodaira, Mt. Tateyama, Japan. *Geochemical Journal*, **47:** 663-673.

Huhn, G., Schulz, H., Stärk, H.-J., Tölle, R. and G. Schüürmann (1995). Evaluation of Regional Heavy Metal Deposition by Multivariate Analysis of Element Contents in Pine Tree Barks. *Water, Air and Soil Pollution*, **84:** 367-383.

Kapička, A., Kodešová, R., Petrovský, E., Hůlka, Z., Grison, H. and M. Kaška (2011). Experimental Study of Fly-Ash Migration by Using Magnetic Method. *Studia Geophysica et Geodaetica*, **55:** 683-696.

Kawano, S. (1999). Disturbance and Conservation of the Subalpine-Alpine Vegetation and Biota in the Tateyama-Kurobe National Park, the Japan North Alps in Central Honshu, Japan—the Results of Long-Term Monitoring. *Japanese Journal of Ecology*, **49:** 313-320.

Kim, W., Doh, S.-J., Park, Y.-H. and S.-T. Yun (2007). Two-Year Magnetic Monitoring in Conjunction with Geochemical and Electron Microscopic Data of Roadside Dust in Seoul, Korea. *Atmospheric Environment*, **41:** 7627-7641.

Kim, W., Doh, S.-J. and Y. Yu (2009). Anthropogenic Contribution of Magnetic Particulates in Urban Roadside Dust. *Atmospheric Environment*, **43:** 3137-3144.

Kim, W., Doh, S.-J. and Y. Yu (2012). Asian Dust Storm as Conveyance Media of Anthropogenic Pollutants. *Atmospheric Environment*, **49:** 41-50.

Kletetschka, G., Žila, V. and P.J. Wasilewski (2003). Magnetic Anomalies on the Tree Trunks. *Studia Geophysica et Geodaetica*, **47:** 371-379.

Kume, A., Numata, S., Watanabe, K., Honoki, H., Nakajima, H. and M. Ishida (2009). Influence of Air Pollution on the Mountain Forests Along the Tateyama–Kurobe Alpine Route. *Ecological Research*, **24:** 821-830.

Lecoanet, H., Lévêque, F. and S. Segura (1999). Magnetic Susceptibility in Environmental Applications: Comparison of Field Probes. *Physics of the Earth and Planetary Interiors*, **115(3):** 191-204.

Lourenço, A., Sequeira, E., Sant'Ovaia, H. and C. Gomes (2014). Magnetic, Geochemical and Pedological Characterisation of Soil Profiles from Different Environments and Geological Backgrounds near Coimbra, Portugal. *Geoderma*, **213:** 408-418.

Magiera, T., Strzyszcz, Z., Kapicka, A. and E. Petrovsky (2006). Discrimination of Lithogenic and Anthropogenic Influences on Topsoil Magnetic Susceptibility in Central Europe. *Geoderma*, **130:** 299-311.

Maher, B.A. (1988). Magnetic Properties of Some Synthetic Sub-Micron Magnetites. *Geophysical Journal International*, **94:** 83-96.

Matzka, J. and B.A. Maher (1999). Magnetic Biomonitoring of Roadside Tree Leaves: Identification of Spatial and Temporal Variations in Vehicle-Derived Particulates. *Atmospheric Environment*, **33:** 4565-4569.

Mullins, C. (1977). Magnetic Susceptibility of the Soil and Its Significance in Soil Science—A Review. *Journal of Soil Science*, **28:** 223-246.

Nagashima, K., Tada, R., Matsui, H., Irino, T., Tani, A. and S. Toyoda (2007). Orbital- and Millennial-Scale Variations in Asian Dust Transport Path to the Japan Sea. *Palaeogeography, Palaeoclimatology, Palaeoecology*, **247:** 144-161.

Sapkota, B., Cioppa, M. and J. Gagnon (2012). Investigation of the Changes in Magnetic and Chemical Properties of Soil During Plant Growth in a Controlled Environment. *Environmental Earth Sciences*, **65:** 385-399.

Schmidt, A., Yarnold, R., Hill, M. and M. Ashmore (2005). Magnetic Susceptibility as Proxy for Heavy Metal Pollution: A Site Study. *Journal of Geochemical Exploration*, **85:** 109-117.

Sheng-gao, L., Shi-qiang, B., Jing-bo, C. and X. Chuang (2005). Magnetic Properties and Heavy Metal Contents of Automobile Emission Particulates. *Journal of Zhejiang University Science B*, **6:** 731-735.

Shi, R. and M.T. Cioppa (2006). Magnetic Survey of Topsoils in Windsor–Essex County, Canada. *Journal of Applied Geophysics*, **60:** 201-212.

Symons, D.T.A. and M.T. Cioppa (2000). Crossover Plots: A Useful Method for Plotting Sirm Data in Paleomagnetism. *Geophysical Research Letters*, **27:** 1779-1782.

Torii, M. (2005). Environmental Magnetism: A Brief Review. *Journal of Geography*, **114:** 284-295.

Watanabe, K., Saito, Y., Tamura, S., Sakai, Y., Eda, N., Aoki, M., Kawabuchi, M., Yamada, H., Iwai, A. and K. Kawada (2011). Chemical Characteristics of the Snow Pits at Murododaira, Mount Tateyama, Japan. *Annals of Glaciology*, **52:** 102-110.

Yang, T., Liu, Q., Li, H., Zeng, Q. and L. Chan (2010). Anthropogenic Magnetic Particles and Heavy Metals in the Road Dust: Magnetic Identification and Its Implications. *Atmospheric Environment*, **44:** 1175-1185.

Asian Journal of Water, Environment and Pollution

Volume 11 Number 3 **July – September, 2014**

Contents

Editorial i

❑ *Snapshot* ii

The Effect of Rainfall Events on Nakdong River's Water Quality Focused on Kangjung-Koryung Weir Area, Korea
DongSeob Song and Hun-Kyun Bae 1

Study on Application of Conventional and Non-Conventional Methods for Defluoridation of Ground Water
P.K. Roy, P. Naskara, D. Ray, G. Banerjee and A. Majumder 9

Concentration of Lead, Cadmium and Mercury in Common Ponyfish (*Leiognathus equulus*) from East Java Coast, Indonesia and Its Impact on Human Health
Lilik Chudaifah, Bambang Irawan and Agoes Soegianto 17

Solid Phase Bioremediation of Butachlor in Contaminated Soil and Evaluation of Leaching Potential
Shailaja S., M. Rama Krishna and Swamy Venkata Yerramsetty 23

Groundwater Quality of Rajnandgaon City, India
K.S. Patel, R. Sharma, B.L. Sahu, R.K. Patel and L. Matini 31

Assessment of the Physical and Bacteriological Quality of Water in the Halabja-Sulaimani-Kurdistan Region of Iraq
Dana A. Mohammed Barzinji and Dilshad G.A. Ganjo 39

Clear Water Local Scour Around Eccentric Multiple Piers to Shift the Line of Sediment Deposition
Rajib Das, Padmini Khwairakpam, Subhasish Das and Asis Mazumdar 47

Electrochemical Performance of Adjusted $LiMn_{1/3}Ni_{1/3}Co_{1/3}O_2$ Recovered from Low Quality Lithiumion Batteries
O.E. Bankole and Lixu Lei 55

Production of Vermicompost Using Aquatic Macrophytes from Domestic Sewage Pond
A.K. Giri, Vishal K., S. Verma, M.P. Singh and Jitender Kumar 63

Economical and Reliable Method of Water Purification
Anand M. Sharan 71

Association of Ambient Air Quality with Female's Pulmonary Function in Kolkata City, India
Paulomi Das and Pinaki Chatterjee 83

Heavy Metals in Fish Species, Sediment and Surface Water around a Proposed Uranium Mining Area in India
Soma Giri and Gurdeep Singh 89

Environment News Futures 97